

# Physiologically Based Pharmacokinetic Model of Itraconazole and Two of Its Metabolites to Improve the Predictions and the Mechanistic Understanding of CYP3A4 Drug-Drug Interactions<sup>§</sup>

Luna Prieto Garcia, David Janzén, Kajsa P. Kanebratt, Hans Ericsson, Hans Lennernäs, and Anna Lundahl

*Drug Metabolism and Pharmacokinetics; Cardiovascular, Renal and Metabolism (L.P.G., D.J., K.P.K., A.L.) and Quantitative Clinical Pharmacology; Early Clinical Development (H.E.), IMED Biotech Unit, AstraZeneca, Gothenburg, Sweden; and Department of Pharmacy, Uppsala University, Uppsala, Sweden (H.L.)*

Received March 14, 2018; accepted July 27, 2018

## ABSTRACT

Physiologically based pharmacokinetic (PBPK) modeling for itraconazole using a bottom-up approach is challenging, not only due to complex saturable pharmacokinetics (PK) and the presence of three metabolites exhibiting CYP3A4 inhibition, but also because of discrepancies in reported in vitro data. The overall objective of this study is to provide a comprehensive mechanistic PBPK model for itraconazole in order to increase the confidence in its drug-drug interaction (DDI) predictions. To achieve this, key in vitro and in vivo data for itraconazole and its major metabolites were generated. These data were crucial to developing a novel bottom-up PBPK model in Simcyp (Simcyp Ltd., Certara, Sheffield, United Kingdom) for itraconazole and two of its major metabolites: hydroxy-itraconazole (OH-ITZ) and keto-itraconazole (keto-ITZ). Performance of the model was validated using prespecified acceptance criteria against

different dosing regimens, formulations for 29 PK, and DDI studies with midazolam and other CYP3A4 substrates. The main outcome is an accurate PBPK model that simultaneously predicts the PK profiles of itraconazole, OH-ITZ, and keto-ITZ. In addition, itraconazole DDIs with midazolam and other CYP3A4 substrates were successfully predicted within a 2-fold error. Prediction precision and bias of DDI expressed as geometric mean fold error were for the area under the concentration-time curve and peak concentration, 1.06 and 0.96, respectively. To conclude, in this paper a comprehensive data set for itraconazole and its metabolites is provided that enables bottom-up mechanism-based PBPK modeling. The presented model is applicable for studying the contribution from the metabolites and allows improved assessments of itraconazole DDI.

## Introduction

After recommendations to stop the usage of ketoconazole by regulatory agencies (CDER, 2013; CHMP, 2013), itraconazole has emerged as one of the best candidates to use as a standard CYP3A4 inhibitor in drug-drug interaction (DDI) studies (CDER, 2017a). Nevertheless, relatively limited experience exists for itraconazole in clinical DDI studies and the optimal study design remains to be defined (Liu et al., 2016). Itraconazole is classified as a class II drug according to the biopharmaceutical drug disposition classification system; it is highly permeable and undergoes more than 90% metabolism (Benet et al., 2011). Itraconazole and its metabolites exhibit complex DDI mechanisms since all act both as CYP3A4 substrates and inhibitors affecting their own metabolic clearance (CL) and that of other drugs. Three major metabolites are sequentially formed by CYP3A4 metabolism: hydroxy-itraconazole (OH-ITZ); keto-itraconazole (keto-ITZ); and *N*-desalkyl itraconazole (ND-ITZ) (Supplemental Fig. 1) (Isoherranen et al., 2004).

A physiologically based pharmacokinetic (PBPK) model for itraconazole is clearly beneficial for both DDI risk assessment and optimization of clinical trial design (Rowland et al., 2011; Liu et al., 2016). An advantage with a PBPK model for itraconazole and its metabolites is the possibility of bringing all information into one model with respect to drug-specific factors (e.g., CYP3A4 affinity, CYP3A4 inhibition, distribution, etc.) in addition to physiological factors. This complexity cannot be intuitively captured by simpler models. Simcyp software (Simcyp Ltd., Certara, Sheffield, United Kingdom) is an established PBPK modeling and simulation tool and has been used in this publication to develop the itraconazole PBPK model presented herein (Rostami-Hodjegan et al., 2012). Three different approaches to develop PBPK models have previously been described and discussed: the bottom-up, top-down, and middle-out approaches (Jamei et al., 2009; Rostami-Hodjegan, 2012; Tsamandouras et al., 2015). Briefly, the bottom-up approach is based on in vitro-in vivo extrapolation techniques, which allow mechanistic extrapolation from in vitro and in silico data to human pharmacokinetics (PK). In the top-down approach parameters are optimized with respect to observed clinical data but the predictive utility of such models may be limited by issues such as parameter

<https://doi.org/10.1124/dmd.118.081364>.

<sup>§</sup>This article has supplemental material available at [dmd.aspetjournals.org](http://dmd.aspetjournals.org).

**ABBREVIATIONS:** ACN, acetonitrile; AUC, area under the plasma concentration-time curve; CL, clearance; CL<sub>R</sub>, renal clearance; DDI, drug-drug interaction; DMSO, dimethylsulfoxide; EAC, enzyme activity change; *f*<sub>1</sub>, difference factor; *f*<sub>u,mic</sub>, fraction of unbound drug in microsomal incubation; *f*<sub>u,p</sub>, fraction of unbound drug in plasma; GMFE, geometric mean fold error; HLM, human liver microsomes; keto-ITZ, keto-itraconazole; *K*<sub>i</sub>, constant of inhibition; *K*<sub>m</sub>, Michaelis constant; LC-MS/MS, liquid chromatography–tandem mass spectrometry; MDCM, multiple depletions curve method; ND-ITZ, *N*-desalkyl itraconazole; NLME, nonlinear mixed effect; OH-ITZ, hydroxy-itraconazole; PBPK, physiologically based pharmacokinetic; PK, pharmacokinetics; SAC, single adjustable compartment; SI, sensitivity index; *v*<sub>max</sub>, theoretical maximum depletion rate; *V*<sub>ss</sub>, volume of distribution.

identifiability and model misspecification. The middle-out approach is a combination of the other two.

Several challenges hinder the development of PBPK models for itraconazole. First, the complex PK with saturable CYP3A4 metabolism and inhibition presents a challenge. All three metabolites are potent CYP3A4 inhibitors and their contribution to clinical DDIs has been considered relevant in a first assessment using static equations (Templeton et al., 2008). Second, there is a lack of robust in vitro data in the literature, which causes uncertainty when building a mechanistic PBPK model based on a bottom-up approach (Chen et al., 2016). Large variabilities in reported in vitro data are mainly due to solubility issues and high protein binding for itraconazole itself as well as its metabolites (Heykants et al., 1989; Isoherranen et al., 2004). The existing itraconazole PBPK library model in Simcyp includes only one metabolite (OH-ITZ) and tends to overpredict the DDI risk (Marsousi et al., 2018). Although Chen et al. (2016) recently published a PBPK model for itraconazole and OH-ITZ using a top-down approach to overcome the challenges of obtaining robust in vitro data from the literature, it is important to continue the efforts of producing robust in vitro data to further develop a more mechanistic PBPK model and this has been emphasized previously for itraconazole (Chen et al., 2016). We believe that further improvements to existing PBPK models are needed, ideally including all metabolites to assess in depth their contribution to the DDI. One limitation with the software selected for our PBPK model is that it is only possible to have two metabolites included. Given the sequential formation of the metabolites, OH-ITZ and keto-ITZ were included in our model and in vitro data for ND-ITZ was generated to be incorporated in future models.

The overall objective of this study is to provide a comprehensive mechanistic PBPK model for itraconazole to increase the confidence in its DDI predictions. To achieve this, key in vitro and in vivo data for itraconazole and its major metabolites were generated, providing improved PK knowledge. These new data were crucial to the development of a bottom-up PBPK model for itraconazole incorporating for first time two of its major metabolites: OH-ITZ and keto-ITZ. Thus, in this paper we provide a comprehensive data set for itraconazole and its three metabolites. This data set enables the development of a bottom-up mechanistic PBPK model that is applicable of assessing clinical itraconazole DDIs and studying the contribution from its metabolites to the DDI.

## Materials and Methods

### Clinical Data Collection

A total of 11 clinical studies, previously collected by Chen et al. (2016), were used for PK profile verification of itraconazole and OH-ITZ. Two studies included

data for keto-ITZ and were used for model verification of this metabolite (Templeton et al., 2008; Liang et al., 2016). Plasma concentration-time profiles and variability were extracted from the figures in the publications. A total of 18 DDI studies using itraconazole as a CYP3A4 inhibitor were used for model validation. Ten clinical DDI studies including midazolam as the substrate have been reported and previously collected by Chen et al. (2016). Eight DDI studies involving other CYP3A4 substrates previously collected by Marsousi et al. (2018) were also used. Different dosing regimens, such as single or multiple dosing with oral solution or capsule formulation of itraconazole were given in these studies. Detailed clinical trial information including original references and the simulated trial designs are described in Tables 1 and 2.

### Experimental In Vitro Determination

**Materials.** Itraconazole stock solutions in dimethylsulfoxide (DMSO) (10 mM) were obtained from the AstraZeneca Compound Management. OH-ITZ, keto-ITZ, and ND-ITZ were purchased from Toronto Research Chemical (Toronto, Canada). Ultra-Pool human liver microsomes (HLM) (mixed gender, lot no. 38289) were purchased from BD Gentest (San Jose, CA). NADPH and phosphate-buffered saline (pH 7.4) were obtained from Sigma (St. Louis, MO). Human blood from three donors was purchased from Bioreclamation VT (New York City, NY). A rapid equilibrium dialysis device was procured from Thermo Fisher Scientific (Waltham, MA). Midazolam was purchased from International Laboratory (San Francisco, CA). Recombinant CYP3A4 enzymes were acquired from Cypex (Dundee, United Kingdom).

**Human and Rat Plasma Protein Binding.** Equilibrium dialysis in human and rat plasma using the rapid equilibrium dialysis device was performed to measure the fraction of unbound drug in plasma ( $f_{u,p}$ ) in human and rat plasma. First, 300  $\mu$ l plasma and 500  $\mu$ l phosphate buffer (pH 7.4) were added to the two separate chambers of the device. A stock solution of compound in DMSO was added into the plasma compartment to yield a final drug concentration of 5  $\mu$ M and final percent volume of DMSO of 0.5%. The compounds were dialyzed for 18 hours at 37°C while shaking at 500 rpm in an air incubator. After completion of dialysis, plasma and buffer samples were quenched with acetonitrile (ACN), diluted, and analyzed by liquid chromatography–tandem mass spectrometry (LC-MS/MS). Calculations of  $f_{u,p}$  in plasma were performed as previously described (Wan and Rehnrgren, 2006).

**Fraction Unbound in HLM Incubations.** Equilibrium dialysis was performed to determine the fraction unbound drug in microsomal incubation ( $f_{u,mic}$ ) in HLM (1 mg/ml in 0.1 M phosphate buffer, pH 7.4) as previously described (Chen et al., 2017). First, 150  $\mu$ l of HLM and 150  $\mu$ l phosphate buffer (0.1 M, pH 7.4) were added to the two separate chambers of the dialysis device. Following 60 minutes of preincubation at 37°C, the compound was added to the HLM chamber. The compounds were dialyzed for 4 hours (37°C, 300 rpm). After completion of dialysis, HLM and buffer samples were quenched with ACN, diluted and analyzed by LC-MS/MS. The DMSO concentration did not reach more than 0.5% of the total incubation volume. Calculations of  $f_{u,mic}$  in HLM were calculated as previously described (Wan and Rehnrgren, 2006).

TABLE 1  
Clinical study data used in the PBPK model development and verification

Data Set	Number <sup>a</sup>	Route	Dose	Regimen	Itraconazole Formulation	Fasted/Fed	PK Data Used in PBPK model	Reference
			mg					
1	6	Oral	100	Once daily $\times$ 7 days	Solution	Fasted	Development; verification	Templeton et al. (2008)
2	3	Oral	200	Once daily $\times$ 11 days	Solution	Fasted	Verification	Liang et al. (2016)
3	14	Oral	200	Once daily $\times$ 15 days	Solution	Fed/Fasted	Verification	Barone et al. (1998)
4	6	Oral	100	Once daily $\times$ 15 days	Capsule	Fed	Verification	Van Peer et al. (1989)
5	5	Oral	100	Once daily $\times$ 15 days	Capsule	Fed	Verification	Hardin et al. (1988)
6	10	Oral	100	Once daily $\times$ 4 wks	Capsule	Fed	Verification	Heykants et al. (1989)
7	10	Oral	200	Once daily $\times$ 4 days	Capsule	Fasted	Verification	Ohkubo and Osanai (2005)
8	8	Oral	200	Once daily $\times$ 6 days	Capsule	Fasted	Verification	Uno et al. (2006)
9	6	Oral	200	Once daily $\times$ 10 days	Capsule	Fasted	Verification	Miura et al. (2010)
10	28	Oral	200	Twice daily $\times$ 15 days	Capsule	Fed	Verification	Barone et al. (1993)
11	5	Oral	200	Twice daily $\times$ 15 days	Capsule	Fed	Verification	Hardin et al. (1988)

<sup>a</sup>Refers to the number of healthy volunteers in the clinical study reported.

TABLE 2  
Comparison between predicted and observed clinical DDI studies

Data Set	Itraconazole	CYP3A4 Substrate	Substrate Dose Regimen	Predicted DDI Ratio <sup>a</sup>		Observed DDI Ratio		Model Validation Predicted/Observed		Reference
				AUC <sup>b</sup>	C <sub>max</sub> <sup>b</sup>	AUC <sup>b</sup>	C <sub>max</sub> <sup>b</sup>	AUC <sub>R</sub> <sup>c</sup>	C <sub>maxR</sub> <sup>c</sup>	
12	200 mg once daily × 4 days, capsule	Midazolam	7.5 mg, day 4, 1 h post-ITZ	8.9	3.0	10.8	3.4	0.8	0.9	Templeton et al. (2010)
13	100 mg once daily × 4 days, capsule	Midazolam	7.5 mg, day 4, 2 h post-ITZ	5.0	2.7	5.7	2.5	0.9	1.1	Templeton et al. (2010)
14	200 mg once daily × 1 day, capsule	Midazolam	7.5 mg, day 1, 2 h post-ITZ	6.4	2.7	3.4	1.8	1.9	1.5	Templeton et al. (2010)
15	200 mg once daily × 4 days, capsule	Midazolam	0.05 mg, IV, day 4, 2 h post-ITZ	3.6	1.1	3.2		1.1		Oikkola et al. (1996)
16	200 mg once daily × 6 days, capsule	Midazolam	7.5 mg, day 6, 2 h post-ITZ	8.6	2.7	6.6	2.5	1.3	1.1	Oikkola et al. (1996)
17	200 mg once daily × 4 days, capsule	Midazolam	7.5 mg, day 4, 2 h post-ITZ	7.6	2.7	8.0	3.1	0.9	0.9	Ahonen et al. (1995)
18	200 mg once daily × 4 days, capsule	Midazolam	7.5 mg, day 8, 4 days post-ITZ <sup>d</sup>	1.3	1.0	2.6	1.9	0.5	0.5	Oikkola et al. (1996)
19	50 mg single dose, solution	Midazolam	2 mg, 4 h post-ITZ <sup>e</sup>	2.5	1.7	2.0		1.2		Backman et al. (1998)
20	200 mg single dose, solution	Midazolam	2 mg, 4 h post-ITZ <sup>e</sup>	6.8	2.6	4.7		1.4		Backman et al. (1998)
21	400 mg single dose, solution	Midazolam	2 mg, 4 h post-ITZ <sup>e</sup>	10.7	2.8	5.4		2.0		Oikkola et al. (1994)
22	200 mg once daily × 4 days, capsule	Simvastatin	40 mg, day 4, 2 h post-ITZ	18.4	10.1	19	17	1.0	0.6	Neuvonen et al. (1998)
23	200 mg once daily × 4 days, capsule	Triazolam	0.25 mg, day 4, 1 h post-ITZ	8.6	2.6	19 <sup>f</sup>	2.5 <sup>f</sup>	0.5	1.0	Varhe et al. (1994)
24	200 mg single dose, capsule	Triazolam	0.25 mg, simultaneously with ITZ <sup>e</sup>	7.2	2.6	3.1	1.4	2.3	1.9	Neuvonen et al. (1996)
25	200 mg single dose, capsule	Triazolam	0.25 mg, 3 h post-ITZ <sup>e</sup>	5.5	2.4	4.5	1.8	1.2	1.3	Neuvonen et al. (1996)
26	200 mg single dose, capsule	Triazolam	0.25 mg, 12 h post-ITZ <sup>e</sup>	2.9	1.9	4.3	1.8	0.7	1.0	Neuvonen et al. (1996)
27	200 mg single dose, capsule	Triazolam	0.25 mg, 24 h post-ITZ <sup>e</sup>	2.0	1.4	3.8	1.7	0.5	0.8	Neuvonen et al. (1996)
28	200 mg once daily × 6 days, capsule	Alprazolam	0.8 mg, day 4, 1 h post-ITZ	2.4	1.0	2.7	1.2	0.9	0.9	Yasui et al. (1998)
29	100 mg once daily × 4 days, capsule	Quinidine	100 mg, day 4, 1 h post-ITZ	3.5	1.4	2.4	1.6	1.4	0.8	Kaukonen et al. (1997)
							GMFE	1.06	0.96	

ITZ, itraconazole.  
<sup>a</sup>All predicted AUC ratios are presented as the geometric mean.  
<sup>b</sup>The AUC and C<sub>max</sub> ratios presented are for the CYP3A4 substrate with and without the presence of itraconazole.  
<sup>c</sup>AUC<sub>R</sub> and C<sub>maxR</sub> refer to the ratio between predicted vs. observed AUC or C<sub>max</sub> ratios.  
<sup>d</sup>Evaluation after 4-day washout of itraconazole.  
<sup>e</sup>Evaluation after a single dose of itraconazole.  
<sup>f</sup>The AUC and C<sub>max</sub> ratios were calculated from the published data.

**Substrate Depletion Experiment.** A substrate depletion method was used to identify the enzyme kinetic parameters: the maximum velocity of the metabolic reaction ( $V_{\max}$ ) and the Michaelis constant ( $K_m$ ) of itraconazole, OH-ITZ, keto-ITZ, and ND-ITZ. Itraconazole and its metabolites were incubated at 37°C 600 rpm with recombinant CYP3A4 enzymes (15 nM). All experiments were optimized for protein and time to ensure linearity and run at different test occasions ( $n = 3$ ). Substrates were added to incubations from a 50 nM stock solution in 90% ACN. Nominal substrate concentrations in the final incubation were 5, 10, 20, 40, 80, 160, 320, and 500 nM and the total ACN content in the incubation mixture did not exceed 0.1%. After preincubation for 5 minutes, the reaction was initiated with NADPH to a final concentration of 1 mM. At time points 1, 2, 3.5, 5, 10, and 15 minutes, 15  $\mu$ l samples were quenched with 30  $\mu$ l of ice-cold ACN. Then, samples were centrifuged (3220g at 4°C for 30 minutes) and supernatant was transferred and diluted for analysis by LC-MS/MS.

**Calculation of Enzyme Kinetics Parameters.** The  $K_m$  and  $V_{\max}$  values were determined according to the multiple depletions curve method (MDCM) described by Sjögren et al. (2009). The model including enzyme activity change (EAC) was selected (eq. 1). The variable EAC was described as monoexponential decay (MDCM + EAC constant), taking into account potential enzyme degradation and/or inhibition effects during the incubation period:

$$-\frac{d[C]}{dt} = v = \left( \frac{v_{\max} \cdot [C]}{K_m + [C]} \right) \cdot e^{-k_e \cdot t} \quad (1)$$

where  $v_{\max}$  is the theoretical maximum depletion rate;  $K_m$  is the substrate concentration at one-half the  $v_{\max}$ ;  $[C]$  is the substrate concentration; and  $k_e$  is the EAC constant. The parameters,  $v_{\max}$  and  $K_m$ , were estimated by simultaneous fitting of the equation to all concentration-time profiles using the nonlinear mixed effect (NLME) in Phoenix NLME 15 version 6.0 (Pharsight Corporation, A Certara Company, Princeton, NJ). The  $V_{\max}$  value was obtained by dividing  $v_{\max}$  by the protein concentration used in the incubation ( $C_p$ ):

$$V_{\max} = \frac{v_{\max}}{C_p} \quad (2)$$

**CYP3A4 Inhibition Assay.** The inhibition parameter describing the inhibitor concentration that reduces the enzyme activity by 50% (the  $IC_{50}$  value) for itraconazole, OH-ITZ, keto-ITZ, and ND-ITZ in HLM was measured using 1'-hydroxylation of midazolam as a probe reaction for CYP3A4-mediated metabolism. The incubations were performed with 0.2 mg/ml pooled HLM in 100 mM phosphate buffer (pH 7.4) with 1 mM EDTA and a total concentration of 1 mM NADPH ( $n = 3$ ). The midazolam concentration was 3  $\mu$ M. The optimal substrate conditions were previously internally validated. Itraconazole, OH-ITZ, keto-ITZ, and ND-ITZ were added at nominal concentrations of 0, 3, 10, 30, 100, 300, and 1000 nM. The final concentration of DMSO:ACN was 0.3:0.7% v/v. A time-zero sample was collected after preincubation for 5 minutes at 37°C and the reaction was initiated by the addition of NADPH. A second sample was taken after a 5-minute incubation. All samples were quenched with ice-cold ACN (1:1). Then, the samples were centrifuged (3220g for 30 minutes) and supernatant was transferred and diluted for analysis by LC-MS/MS.

The  $IC_{50}$  value was determined by fitting the experimental data to an  $I_{\max}$  model (eq. 3) using Phoenix NLME:

$$E = E_0 \cdot \left( 1 - \frac{C}{IC_{50} + C} \right) \quad (3)$$

where  $E$  is the effect of inhibition;  $E_0$  is the baseline; and  $C$  is the concentration of substrate. The constant of inhibition ( $K_i$ ) was calculated by a classic competitive inhibition model described in eq. 4:

$$K_i = \frac{IC_{50}}{\left[ \frac{S}{K_m(\text{mdz})} + 1 \right]} \quad (4)$$

where  $S$  is the concentration in the incubation and  $K_m(\text{mdz})$  is the Michaelis constant of midazolam (2  $\mu$ M) (Cer et al., 2009).

**Pharmacokinetic Study of Intravenous Administration in Rat.** Male Han Wistar rats ( $n = 2$ , ~300 g) (Charles River, Sulzfeld, Germany), were dosed with keto-ITZ solution (1 mg/kg, 1 ml/kg, bolus) intravenously into the tail vein. The formulation was 5% DMSO and 95% 2-hydroxypropyl-beta-cyclodextrin

(30% w/v) in water adjusted to pH 4. Blood samples were collected into EDTA-coated tubes at 2, 7, 15, 30, 60, 120, 240, 360, 420, and 1440 minutes after dose. Urine samples were also collected during the following intervals 0–120, 120–360, and 360–1440 minutes after dose. All samples were centrifuged at 3220g for 5 minutes at 4°C. Blood samples were immediately stored in polypropylene tubes at  $-80^\circ\text{C}$  and deproteinated by solvent precipitation prior to analysis. Samples were diluted for analysis by LC-MS/MS. The PK parameters were estimated by one-compartmental analyses using Phoenix NLME.

Before the study, the animals were acclimatized for a minimum of 3 days and allowed food and water ad libitum. All of the animal studies were conducted in accordance with the National Institutes of Health guidelines on animal welfare.

## Model Acceptance Criterion for PK Verification and DDI Validation

The following criteria were predetermined to assess model performance. First, the performance of the model in describing the PK profiles of itraconazole, OH-ITZ, and keto-ITZ was verified if the observed concentration-time profiles were within the 90% prediction interval (5th to 95th percentile range of the virtual population). Following the verification of the PK model for itraconazole and its metabolites, simulations were performed to test the capability of the model to accurately describe DDI studies with itraconazole and midazolam. The geometric mean area under the plasma concentration-time curve (AUC) ratio for each DDI study was determined and the predicted and observed data were compared (see Table 2 for results). Precision and bias for the DDI predictions were evaluated using the geometric mean fold error (GMFE) described in eq. 5:

$$GMFE = 10^{\sum \log(\text{Predicted DDI}/\text{Observed DDI}) / \text{Number of predictions}} \quad (5)$$

To assess the predictive performance and ensure no bias and good precision of DDI, the predicted/observed ratio for AUC and  $C_{\max}$  should be within a predefined criterion of a 2-fold range and the GMFE should be between 0.85 and 1.25. To further strengthen the final model predictive performance, an additional validation including other CYP3A4 substrates was also performed. The details of the studies used are listed in Table 2.

## PBPK Parameter Input and Model Development

A full PBPK model was constructed for itraconazole and its metabolites (OH-ITZ and keto-ITZ) using mainly a bottom-up approach (Jamei et al., 2009) in Simcyp. Key parameters (i.e.,  $f_{u,p}$ ,  $f_{u,mic}$ ), enzyme kinetics, and CYP3A4 inhibition were redefined using the in vitro data presented in this paper (Table 3). The overall model development, verification, and validation process is presented in Fig. 1.

The physicochemical properties for itraconazole and OH-ITZ were used as described in the compound library files. The  $f_{u,p}$  value for itraconazole was set to 0.01 according to US Food and Drug Administration guidelines. For keto-ITZ, where no previous model was available, the physicochemical parameters were calculated from its chemical structure using the Biobyte software, version 4.3 (Pomona College and BioByte, Inc., Claremont, CA). The blood-to-plasma ratio and  $pK_a$  were assumed to be the same as the parent. All values are listed in Table 3.

The first-order absorption model for itraconazole was used keeping the fraction absorbed and the absorption constant as in the software library. The values were adjusted when clinical studies with solutions or capsule formulations were simulated (Table 3). A nominal flow in the gut model was predicted using the Simcyp toolbox and the fraction unbound drug in the gut was assumed to be the same as  $f_{u,p}$  in plasma.

For the volume of distribution ( $V_{ss}$ ) parameter, a full PBPK model was used to reach predefined values for itraconazole and OH-ITZ. Method 1, described originally by Poulin and Theil (2009), was selected for prediction of the tissue-to-plasma partition coefficients for individual tissues. The  $V_{ss}$  value for itraconazole was taken from Mouton et al. (2006). The  $V_{ss}$  values for OH-ITZ and keto-ITZ were scaled from rat (Yoo et al., 2000) to human using the Oie-Tozer method (Oie and Tozer, 1979). A minimal PBPK model was used for keto-ITZ since a full PBPK model is not currently available for the second metabolite in the software. The addition of a single compartment was used to describe the two-compartmental behavior of the plasma PK profiles of keto-ITZ. The single adjustable compartment (SAC) parameters, the SAC volume, first-order rate constant for the distribution to a SAC, and first-order rate constant for the distribution from a SAC, were determined by best fit using data set 1 on day 1. The parameters used in the model are listed in Table 3.

TABLE 3  
Input drug-dependent parameter values used for itraconazole and its metabolites in the PBPK model

Parameter	Itraconazole		OH-Itraconazole		Keto-Itraconazole	
	Value	Reference	Value	Reference	Value	Reference
MW (g/mol)	705.6	Library V15 <sup>a</sup>	721.6	Library V15 <sup>a</sup>	719.6	Calculated <sup>b</sup>
Log P <sub>ow</sub>	4.47	Library V15 <sup>a</sup>	4.64	Library V15 <sup>a</sup>	4.98	Calculated <sup>b</sup>
pK <sub>a</sub>	4.28	Library V15 <sup>a</sup>	4.28	Library V15 <sup>a</sup>	4.28	Assumed same as parent
B/P	0.58	Library V15 <sup>a</sup>	0.58	Library V15 <sup>a</sup>	0.58	Assumed same as parent
f <sub>up</sub> <sup>c</sup>	0.01	FDA <sup>d</sup>	0.012	Internally measured <sup>e</sup>	0.01	Internally measured <sup>e</sup>
Absorption model						
f <sub>a</sub>	1/0.59	Sol/Cap Library V15 <sup>a</sup> (first order)				
K <sub>a</sub> (h <sup>-1</sup> )	1.5/0.6	Sol/Cap Library V15 <sup>a</sup> (first order)				
f <sub>u,gut</sub>	0.01	Assumed same as f <sub>u,p</sub> (first order)	0.012	Assumed same as f <sub>u,p</sub>	0.01	Assumed same as f <sub>u,p</sub>
MDCK II (10 <sup>-6</sup> cm/s)	57.1	Library V15 <sup>a</sup> (first order)				
Q <sub>gut</sub> (l/h)	15.7	Simcyp predicted				
Distribution model						
V <sub>ss</sub> (l/kg)	3.9	Mouton et al. (2006) (full PBPK)	3.8	Scaled from Rat <sup>f</sup> (full PBPK)	5.2	Scaled from Rat <sup>f</sup> (minimal PBPK + SAC; internally measured <sup>e</sup> )
Elimination						
V <sub>sac</sub> (l/kg)						
k <sub>ip</sub> /k <sub>out</sub> (h-1)						
Additional CL (l/h)						
V <sub>max</sub> CYP3A4 (pmol/min per picomoles isoform)	5.31	Internally measured <sup>e</sup>	1.66	Internally measured <sup>e</sup>	38.9	Scaled from Rat (Internally measured <sup>d</sup> )
K <sub>m</sub> CYP3A4 (μM)	0.28	Internally measured <sup>e</sup>	0.11	Internally measured <sup>e</sup>	1.84	Internally measured <sup>e</sup>
f <sub>u,mic1</sub>	0.19	Internally measured <sup>h</sup>	0.65	Internally measured <sup>h</sup>	0.08	Internally measured <sup>e</sup>
System (ISEF)	0.25	Cypex HR	0.25	Cypex HR	0.61	Internally measured <sup>e</sup>
CL <sub>R</sub> (l/h)	0	Library V15 <sup>a</sup>	1.39	Library V15 <sup>a</sup>	0.25	Cypex HR
Hepatic uptake	1		1		0.18	Scaled from Rat (Internally measured <sup>e</sup> )
Cytochrome P450 inhibition						
K <sub>i</sub> CYP3A4 (μM)	0.038	Internally measured <sup>e</sup>	0.042	Internally measured <sup>e</sup>	0.037	Internally measured <sup>e</sup>
f <sub>u,mic2</sub>	0.01	Internally measured <sup>e</sup>	0.076	Internally measured <sup>e</sup>	0.063	Internally measured <sup>h</sup>

B/P, blood-to-plasma ratio; f<sub>a</sub> fraction of dose absorbed; FDA, US Food and Drug Administration; f<sub>u,gut</sub> fraction of unbound drug in the gut; HR, high reductase; ISEF, inter system extrapolation factor for scaling of recombinant CYP in-vitro kinetic data; K<sub>a</sub>, absorption constant; k<sub>in</sub>, first-order rate constant for the distribution to a single adjustable compartment; k<sub>out</sub>, first-order rate constant for the distribution from a single adjustable compartment; MW, molecular weight; Q<sub>gut</sub>, nominal flow through the gut; V<sub>sac</sub>, SAC volume.

<sup>a</sup>Refers to the Simcyp simulator compound library (version 15).

<sup>b</sup>Determined using software Biobyte (Pomona College and BioByte, Inc.).

<sup>c</sup>All compounds are monocrotic base (Simcyp Library version 15).

<sup>d</sup>The US Food and Drug Administration recommends that of f<sub>u,p</sub> should be set to 0.01 if experimentally determined to be <0.01 (US Food and Drug Administration Guidance for In Vitro Metabolism- and Transporter- Mediated Drug-Drug Interaction Studies. <http://www.fda.gov/Drugs/GuidanceRegulatoryInformation/Guidances/default.htm>).

<sup>e</sup>Refers to data published in this paper, details in *Materials and Methods*, and values to Table 4.

<sup>f</sup>The V<sub>ss</sub> value was scaled from rat to human using the Oie-Tozer method (Oie and Tozer, 1979). Different rat V<sub>ss</sub> references were used for OH-ITZ (Yoo et al., 2000) and keto-ITZ in-house data (Table 4).

<sup>g</sup>SAC parameters were optimized to match PK profiles at day 1 of data set 1.

<sup>h</sup>Calculated from internally measured f<sub>u,mic</sub> and corrected by protein concentration in the assay (Wan and Rehngrén, 2006).

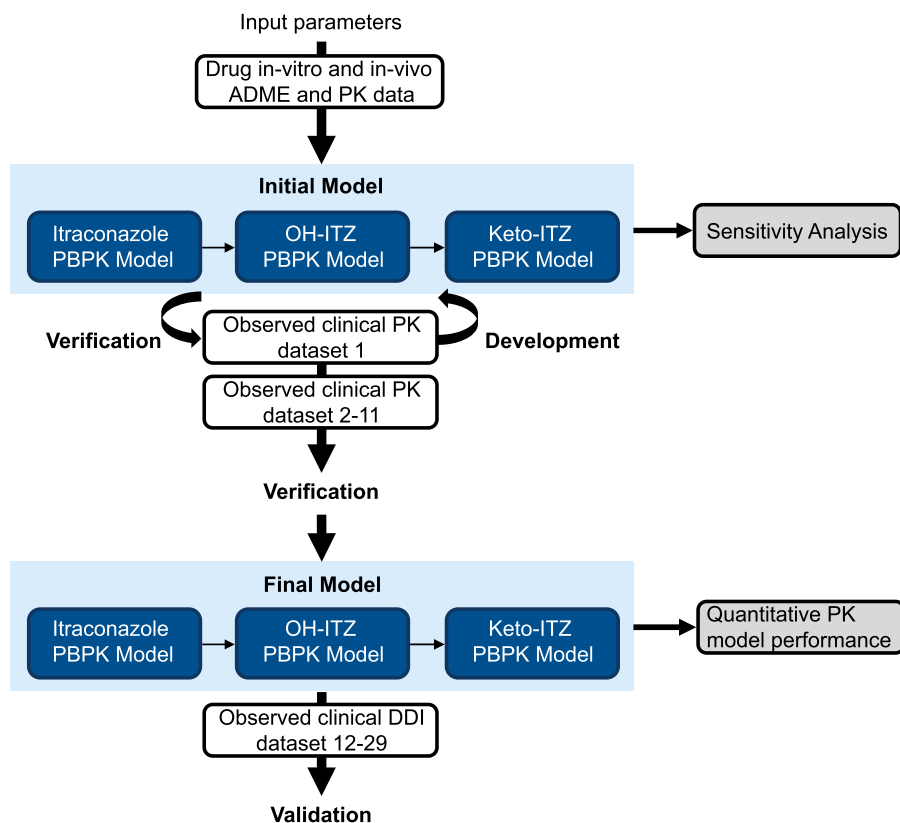


**Fig. 1.** Workflow of the development, verification, and validation of the PBPK model for itraconazole, OH-ITZ, and keto-ITZ.

The hepatic CL for itraconazole and its metabolites was scaled in the model from the CYP3A4 enzyme kinetic parameters  $K_m$  and  $V_{max}$  that were determined by the MDCM method described previously. The renal CL ( $CL_R$ ) for keto-ITZ was scaled from rat using the Simcyp toolbox. In the case of keto-ITZ, CYP3A4 metabolism and  $CL_R$  were not sufficient to describe the observed CL in humans. In addition, unspecific CL was included for this compound to capture a potential alternative route of elimination. The additional CL was added using the retrograde method and the CL determined in rats and scaled to humans was used as the starting value.

The  $f_{u,mic}$  determined by dialysis in microsomal incubation mixtures was incorporated into each model to correct for protein binding in the in vitro experiments. The  $f_{u,mic}$  value was corrected for the protein concentrations used in each assay (Table 3). Specifically, for enzyme kinetics parameters ( $f_{u,mic1}$ ), the method described by Wan and Rehngren (2006) was used. For inhibition parameters ( $f_{u,mic2}$ ), where protein concentration was similar to measured  $f_{u,mic}$  conditions, no correction was deemed necessary based on the binding profile of OH-ITZ (Tran et al., 2002).

### Simulations Using PBPK Modeling

The Simcyp (version 15) population-based PBPK simulator (Simcyp Ltd., Certara) was used to simulate the PK of itraconazole and its metabolites (OH-ITZ and keto-ITZ), and relevant DDI in virtual healthy volunteers. Simulations were performed with randomly selected individuals from a simulated healthy volunteer population built in the Simcyp software (Sim-Healthy). A total of 100 individuals—10 trials with 10 individuals per trial—were simulated to assess variability across groups. The age, sex ratio, dose, formulation, and regimen used in the simulations were matched to the clinical studies described in each trial (Tables 1 and 2). The CYP3A4 substrate models available in the Simcyp compound library were directly used in the simulations. When the DDI simulations were performed, the itraconazole compound file including the two metabolites were put as the substrate file and output was exported to Phoenix. The AUCs from each simulation were calculated by noncompartmental analyses and the log/linear trapezoidal method. The relative contribution of itraconazole and its metabolites (OH-ITZ and keto-ITZ) to the total AUC ratio was calculated following the approach of Wang et al. (2004), where net inhibition is related to the sum of inhibitory contributions of all circulating inhibitors as described in

Templeton et al. (2008). Simulated unbound liver and gut concentrations and the respective apparent  $K_{i,u}$  for itraconazole and its metabolites were used in the calculation. The simulated concentrations were taken from a dosing regimen of once daily administration for 4 days of 200 mg itraconazole (capsule and oral solution) given in the fasted state.

### Model Parameter Sensitivity Analysis

Sensitivity analysis in this context is a description of how sensitive the model is to changes in the model parameters. Key parameters were evaluated in this sensitivity analysis to gain additional insight on their impact on the AUC of itraconazole and its metabolites. The sensitivity analysis was done using two different methods: The one-factor-at-a-time approach and the sensitivity index (SI) approach (Nestorov, 1999; Bonate, 2011). In the one-factor-at-a-time approach, the numerical value of a parameter is varied within a specified region around the estimated optimal parameter value while the change in AUC is observed. The SI for each parameter was calculated using eq. 6:

$$SI = (AUC_{max} - AUC_{min}) / AUC_{max} \quad (6)$$

where  $AUC_{max}$  and  $AUC_{min}$  are the maximum and minimum AUCs, respectively, within the explored parameter space in the sensitivity analysis. The advantage of the SI compared with the one-factor-at-a-time methods is that a direct comparison of the estimated sensitivity of the model parameters is possible.

### Postanalysis of the Simulated Plasma Profiles

To further assess the performance of the model on simulating PK profiles in a quantitative manner, a postanalysis was conducted according to previously established methods (Marston and Polli, 1997). The difference factor ( $f_1$ ), which is a model-independent parameter, was applied for the comparison of the plasma concentration-time profiles of itraconazole, OH-ITZ, and keto-ITZ according to eq. 7:

$$f = \frac{\sum_{i=1}^n |R_i - T_i|}{\sum_{i=1}^n R_i} \cdot 100 \quad (7)$$

where  $n$  is the number of time points, and  $R_i$  and  $T_i$  are the plasma drug concentrations observed and simulated, respectively, at each time point  $t$ .

TABLE 4  
Results from in-vitro and in-vivo experiments

Parameter <sup>a</sup>	Itraconazole	OH-ITZ	Keto-ITZ	ND-ITZ
Human PPB (% free)	0.1 (22%)	1.2 (60%)	1 (39%)	2.9 (23%)
$f_{u,mic}$	0.01 (10%)	0.076 (10%)	0.063 (10%)	0.066 (10%)
$K_m$ CYP3A4 ( $\mu$ M)	0.28 (30%)	0.11 (22%)	0.08 (20%)	0.05 (17)
$V_{max}$ CYP3A4 (pmol/min per picomoles of isoform)	5.31 (26%)	1.6 (17%)	1.84 (16%)	0.99 (12%)
$k_e$ ( $\text{min}^{-1}$ )	0.09 (12%)	0.08 (16%)	0.11 (12%)	0.05 (21%)
$IC_{50}$ ( $\mu$ M)	0.1 (3%)	0.113 (4%)	0.098 (9%)	0.136 (5%)
Apparent $K_i$ ( $\mu$ M) <sup>b</sup>	0.038	0.042	0.04	0.051
Apparent $K_{i,u}$ ( $\mu$ M) <sup>c</sup>	0.0004	0.0032	0.0025	0.0034
Rat $V_{ss}$ (l/kg) <sup>d</sup>	—	—	3.16 (24%)	—
Rat $CL_{iv}$ (ml/min per kilogram) <sup>d</sup>	—	—	79.78 (11%)	—
Rat $CL_R$ (ml/min per kilogram) <sup>d</sup>	—	—	0.04 (18%)	—
Rat PPB (% free)	—	0.61 (17%)	0.43 (18%)	—

$k_e$ , enzyme activity change constant; PPB, plasma protein binding. —, not measured.

<sup>a</sup>All data presented as arithmetic mean and CV (%) ( $n = 3$ ).

<sup>b</sup>Calculated by eq. 4 (Cer et al., 2009).

<sup>c</sup>Calculated by correcting with the measured  $f_{u,mic}$ .

<sup>d</sup>These data represent the arithmetic mean of two animals.

## Results

### Experimental In Vitro Determination

**Human and Rat Plasma Protein Binding.** Human and rat plasma protein binding was assessed using equilibrium dialysis. All test compounds were highly bound to plasma proteins in human and rat resulting in low  $f_{u,p}$  values (0.001–0.029), which are presented in Table 4.

**Fraction Unbound in HLM Incubations.** Protein binding was also determined in HLM incubation mixtures by dialysis for itraconazole, OH-ITZ, keto-ITZ, and ND-ITZ. All of the test compounds were extensively bound and this resulted in overall low  $f_{u,mic}$  values (0.01–0.076). The details are presented in Table 4.

**Enzyme Kinetics Analysis.** The CYP3A4 enzyme kinetic parameters ( $V_{max}$  and  $K_m$ ) for itraconazole, OH-ITZ, keto-ITZ, and ND-ITZ were estimated using the MDCM method. A summary of the resulting parameters is presented in Table 4. All concentration-time profiles and model fits for itraconazole and its three metabolites are presented in Fig. 2. Biphasic depletion curves were observed for all four substrates, and therefore MDCM with EAC was used to take into account potential enzyme depletion or inhibition. All four compounds had low unbound  $K_m$  values, indicating high affinity to CYP3A4.

**CYP3A4 Inhibition.** The potency of the CYP3A4 inhibition for itraconazole, OH-ITZ, keto-ITZ, and ND-ITZ was determined in HLM using midazolam as the substrate. A summary of the resulting parameters ( $IC_{50}$  and  $K_i$ ) is presented in Table 4. The fitted  $IC_{50}$  curves versus a range of inhibitor concentrations are presented in Fig. 3A. In addition, the simulated  $IC_{50}$  curves with remaining midazolam (%) versus calculated free concentrations are presented in Fig. 3B.

**Rat PK.** Rats were intravenously dosed with keto-ITZ with the purpose of obtaining  $V_{ss}$ ,  $CL$ , and  $CL_R$  for this metabolite. The plasma and urine concentration-time curves for the individual animals (Supplemental Fig. 2) and the PK parameters ( $V_{ss}$ ,  $CL$ , and  $CL_R$ ) calculated by noncompartmental analysis are presented in Table 4.

### PBPK Model Development and Verification

The PBPK model for itraconazole, OH-ITZ, and keto-ITZ (Table 3) was first developed and optimized using data set 1 (Table 1) as a training data set in a step-wise manner. The simulated plasma concentration profiles of the training data set met the predefined model acceptance

criteria (observed plasma concentration falling within the 90% prediction interval) (Fig. 4, A, C, and E). Furthermore, the model was verified using a separate test data set of 10 human PK studies including observations at a wide range of time points varying from 1 day up to 4 weeks across a multiple dosings regimen, both for solution and capsule formulation at different doses, and under different fed and fasted conditions. Similar to the training data set, all of the simulated concentration profiles (Fig. 4, B, D, and F; Fig. 6) for the verification studies fell within the acceptance criteria. Accumulation over days was reasonably well captured by the model for all three compounds under all of the different conditions (Figs. 4 and 5).

### Model Parameter Sensitivity Analysis

To gain additional insights into this complex model of a parent compound and two sequential metabolites in which all are substrates and inhibitors of CYP3A4, a sensitivity analysis was conducted to assess the relative importance of the key parameters toward changes in itraconazole, OH-ITZ, and keto-ITZ AUC. In general, the AUCs for all three compounds are more sensitive to elimination kinetics parameters and plasma protein binding than to inhibition constants (Fig. 6). The parameters in Fig. 6, A–C, which have an index above 0.75, have the greatest effect on the AUC of itraconazole and its metabolites. Few of the tested parameters were below SI 0.25, indicating that all have considerable impact on the AUC of itraconazole and its metabolites.

### Postanalysis of the Simulated Plasma Profiles

To further quantify the accuracy of the model in predicting the PK profiles for itraconazole and its metabolites, the  $f1$  (deviation observed vs. predicted at identical time points) was calculated. Overall, the PK profiles were predicted adequately, exhibiting  $f1$  of 43%, 30%, and 52% for itraconazole, OH-ITZ, and keto-ITZ, respectively. In Fig. 7 the predicted versus observed concentrations at the same time points are presented.

### Model Validation: Prediction of Itraconazole DDI

The results of the simulated clinical trials including midazolam and itraconazole are summarized in Table 2 and Fig. 8. Overall, the model meets the prespecified criteria predicting 100% of observed midazolam AUC and  $C_{max}$  ratios within 2-fold (Fig. 8A). In addition, 70% of the simulated midazolam AUC ratios were within 1.5-fold

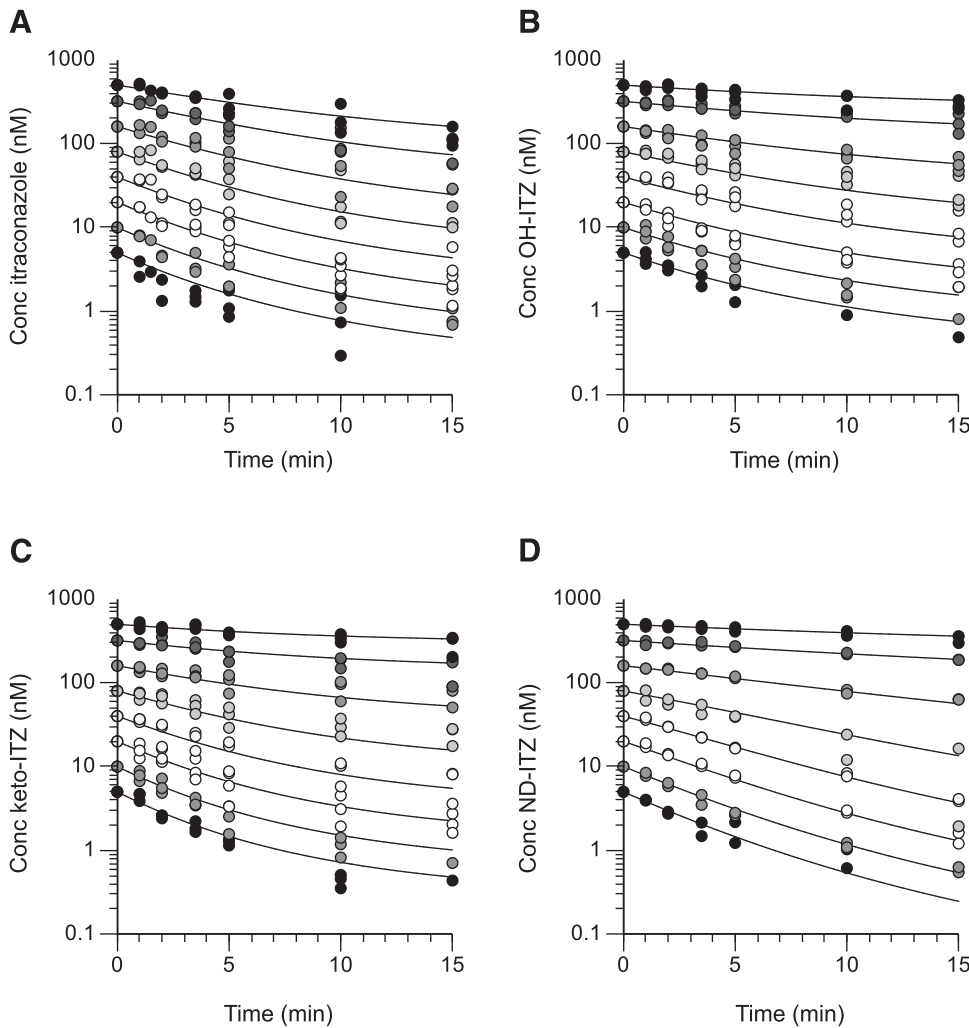


**Fig. 2.** Enzyme kinetic plots using human recombinant CYP3A4. Substrate depletion curves vs. time for eight different initial substrate concentrations (different colors). Circles correspond to observed concentrations. The solid lines represent model fitted data from the NLME modeling using the multiple depletions curves method including correction for loss in enzyme activity for itraconazole (A), OH-ITZ (B), keto-ITZ (C), and ND-ITZ (D).

of the observed data. To further strengthen the DDI validation, other CYP3A4 substrates were also evaluated, confirming the good overall prediction within 2-fold (Fig. 8B; Table 2). The GMFE values were

determined to be 1.06 and 0.96 for the AUC and  $C_{\max}$  ratios, respectively. The GMFE values indicate good precision and no bias when predicting the observed DDI.

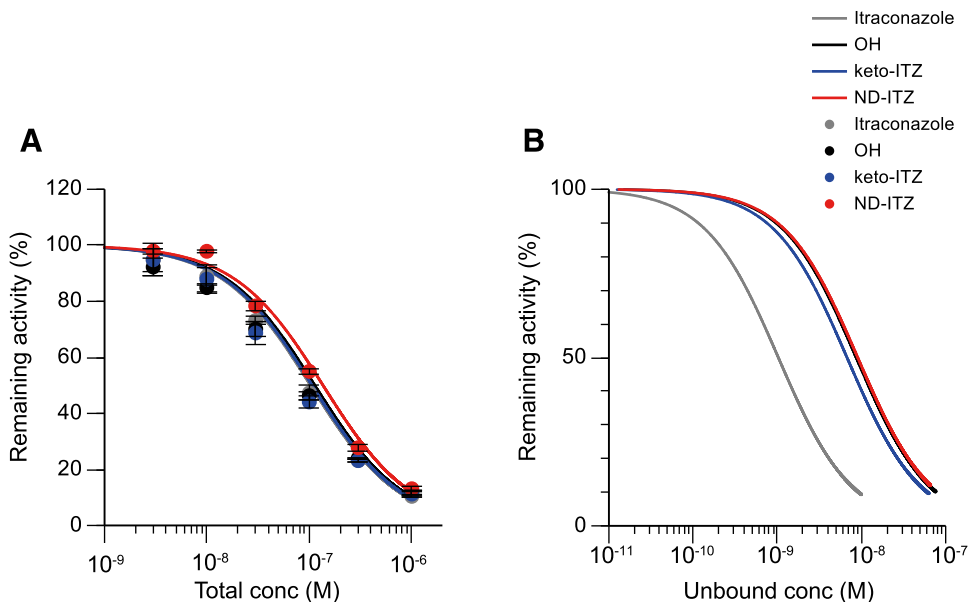


**Fig. 3.** Percentage remaining activity vs. nominal inhibitor concentration using pooled HLM and midazolam hydroxylation as a CYP3A4 probe reaction: itraconazole (gray), OH-ITZ (black), keto-ITZ (blue), and ND-ITZ (red). The circle and error bars correspond to the observed mean data and S.D. The lines in (A) represent the model fitted data; the lines in (B) represent the simulated free concentrations for itraconazole and its metabolites corrected by protein in the incubation.

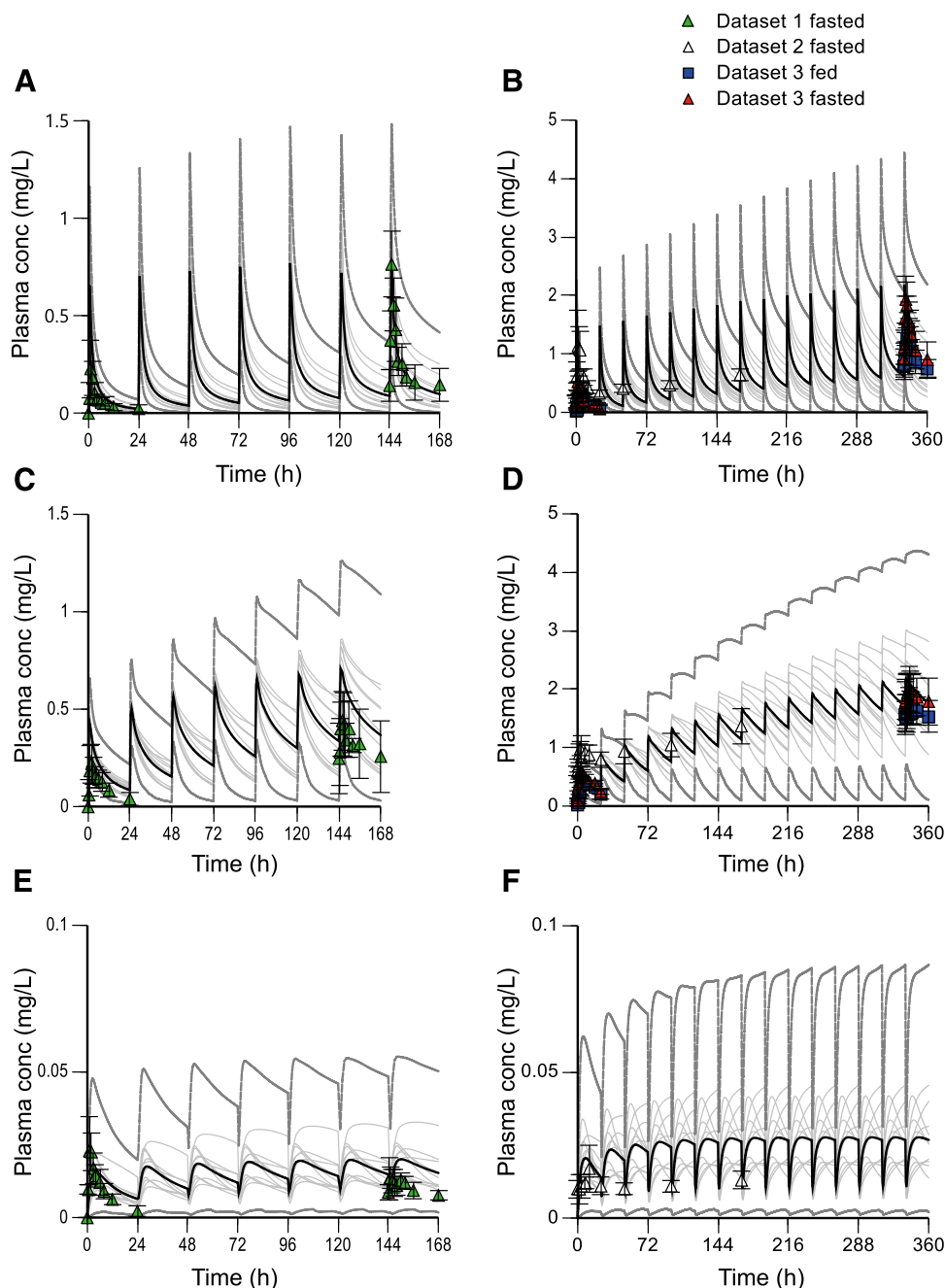


**Fig. 4.** Comparison of plasma concentration-time profiles for itraconazole (A and B), OH-ITZ (C and D), and keto-ITZ (E and F) simulated by PBPK modeling vs. actual clinical data following multiple doses of itraconazole in solution: 100 mg daily dose for 7 days (data set 1) (A, C, and E), and 200 mg daily dose for 11 (data set 2) and 15 days (data set 3) (B, D, and F). The symbols and error bars represent the observed mean data and S.D. from clinical trials. Triangles and squares represent fasted and fed conditions, respectively. The black lines represent the simulated population mean plasma concentration-time profiles (100 individuals), the gray lines represent the simulated mean per trial (10 trials), and the dotted gray lines represent the 90th confidence interval.

#### Model Application: Relative Contribution to the AUC Ratio

The predicted time course of CYP3A4 inhibition after itraconazole dosing using different formulations was simulated (Supplemental Figs. 3 and 4). The figures illustrate the relationship between simulated unbound liver and gut concentrations and the respective unbound apparent  $K_i$  for itraconazole and its metabolites. The corresponding liver average unbound concentration ( $C_{uss}$ )/ $K_{i,u}$  values (over 96 hours) for itraconazole, OH-ITZ, and keto-ITZ for this dose are 85, 31, and 0.7 for capsule formulation and 200, 62, and 0.85 for oral solution formulation. To gain further insights, the relative contributions of itraconazole and its metabolites to the AUC ratio were calculated and are presented in Fig. 9. In the first hours after dose the main contributor is itraconazole (>80%), but as time passes its contribution equals out to a similar level as OH-ITZ (~55% vs. 40%). The relative role of OH-ITZ increases

with time after itraconazole dosing. The contribution of keto-ITZ is minor throughout the studied 8 day period compared with itraconazole and OH-ITZ (<5%).

#### Discussion

In the present work, an accurate PBPK model was developed that simultaneously predicts the PK profiles for itraconazole, OH-ITZ, and keto-ITZ. The performance of the model was successfully verified against several PK ( $n = 11$ ) and DDI ( $n = 18$ ) studies, which included different dosing regimens, formulations, and CYP3A4 substrates (Tables 1 and 2). This study is the first to generate in vivo PK data for keto-ITZ as well as in vitro PK data for itraconazole and its three major metabolites, enabling the necessary scaling PK parameters for building a PBPK model. The strengths of this itraconazole PBPK model compared

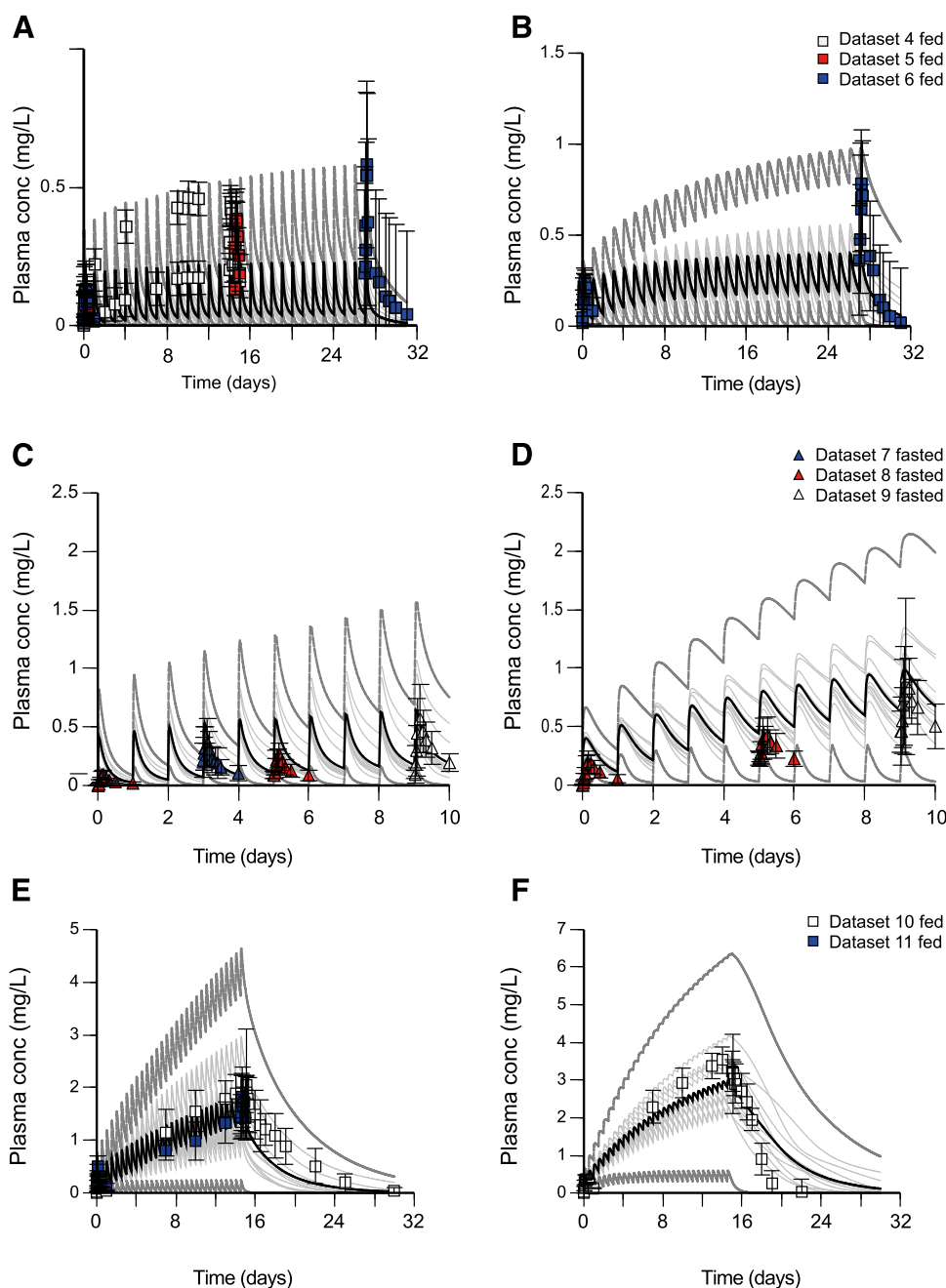


**Fig. 5.** Comparison of plasma concentration-time profiles for itraconazole (A, C, and E) and OH-ITZ (B, D, and F) simulated by PBPK modeling vs. actual clinical data following multiple doses of itraconazole in capsule: 100 mg daily dose in the fed state for 15 days (data sets 4 and 5) and 4 weeks (data set 6) (A and B); 200 mg daily dose in the fasted state for 4, 6, and 1 days (data sets 6, 7, and 8, respectively) (C and D); and 200 mg twice daily in the fed state for 15 days (data sets 10 and 11) (E and F). The symbols and error bars represent the observed mean data and S.D. from clinical trials. Triangles and squares represent fasted and fed conditions, respectively. The black lines represent the simulated population mean plasma concentration-time profiles (100 individuals), the gray lines represent the simulated mean per trial (10 trials), and the dotted gray lines represent the 90th confidence interval.

with previous published are the following: 1) the model includes the second major metabolite of itraconazole, keto-ITZ; 2) the model is built primarily using a bottom-up approach including robust data for inhibition, elimination, and binding parameters; 3) the model includes a sensitivity analysis, which aims to highlight the impact and importance of the parameters included; 4) the model contains a quantitative assessment of model accuracy to predict PK profiles; 5) the model is validated against several CYP3A4 substrates; and 6) the model provides insights into the relative contribution of itraconazole metabolites to the clinical DDI.

The first and most critical step when using PBPK simulations is to accurately predict the PK of the inhibitor and substrate drugs. The model presented meets the prespecified acceptance criteria, with the majority of observed plasma drug concentrations being within the 90% prediction interval (Figs. 4 and 5). Here, the criteria were chosen on the basis of PK

variability of itraconazole and its metabolites derived from its complex PK and bioavailability (Poirier and Cheymol, 1998). Being a drug with a broad therapeutic window (Buchkowsky et al., 2005), more flexible criteria are considered acceptable (Jones et al., 2015). There is a lack of good standardization of model acceptance criteria in PBPK modeling (Sager et al., 2015). Herein, one of the methods highlighted in this review has been used for retrospective analysis together with goodness-of-fit plots following best-practice examples (Wagner et al., 2012; Gertz et al., 2013). The calculation of *f*<sub>1</sub> considers all of the observed data points and is a direct comparison of the predicted value at the specific time point (Fig. 7). The *f*<sub>1</sub> calculations confirm the accuracy in PK predictions for itraconazole (43%) and OH-ITZ (30%) and indicate that the prediction of the PK profile of keto-ITZ is less accurate (53%), following the criteria set by Sjögren et al. (2013). As shown in Fig. 7, precision could be improved for the lower concentrations. On the other

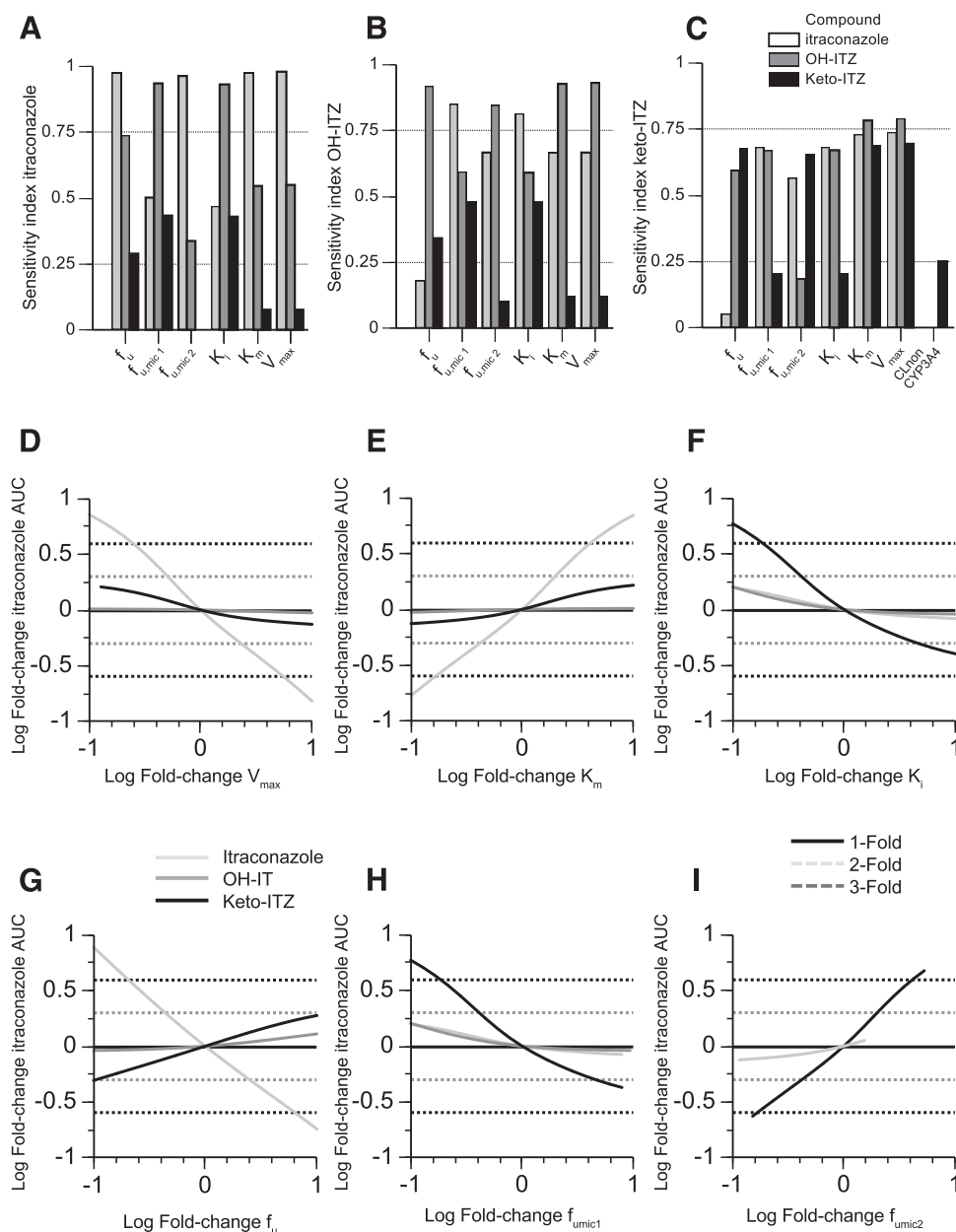


**Fig. 6.** Sensitivity analysis index ratio for the AUC of itraconazole (A), OH-ITZ (B), and keto-ITZ (C). The black horizontal dotted line represents the 0.25 and 0.75 set criteria. Sensitivity analysis on AUC of itraconazole for  $V_{max}$  (D),  $K_m$  (E),  $K_i$  (F),  $f_{u,p}$  (G), and  $f_{u,mic1}$  (H) for  $K_i$ ; and  $f_{u,mic2}$  (I) for enzyme kinetics. Here, the horizontal lines in black represent the 1-fold change in the AUC, the horizontal dotted lines in light gray represent the 2-fold change in AUC, and the horizontal dotted lines in dark gray represent the 4-fold change in AUC. Itraconazole (gray), OH-ITZ (black), and keto-ITZ (blue).

hand, high model performance was observed for  $C_{max}$  and steady-state concentrations of itraconazole (31%) and OH-ITZ (21%).

The second step in the present work was to use the validated PK model to assess how well the model could predict AUC and  $C_{max}$  ratios for CYP3A4 substrates with and without the presence of an inhibitor. In general, the predicted versus observed ratios were within 2-fold (Fig. 8B) with good precision and no bias in the DDI prediction showing GMFE values close to 1. There are some specific scenarios where predictions could be further improved, which could also be observed in the Chen et al. (2016) model when the same studies were simulated. For example, when the itraconazole oral dose reached 400 mg an inhibition plateau was observed on day 1 (Templeton et al., 2010). The model overpredicted the AUC ratio and did not capture the plateau (data set 21). To date, the mechanism behind this plateau is not understood and more clinical studies using the 400 mg itraconazole dose would help to clarify this finding. Another example is the general trend to underpredict the DDI in scenarios where the substrate is given more than 12 hours after

itraconazole dose (data sets 18, 26, and 27); this could be due to the unrecognized contribution of the last metabolite, ND-ITZ. Nevertheless, in the case of itraconazole and clinical study designs for DDI, the most critical data are the steady-state prediction, where our model showed more accurate performance with 89% of these studies within the more strict criteria of 1.5-fold error (i.e., trials 12 to 13, 15–17, 22 to 23, and 28 to 29 in Table 2).

The role of metabolites in DDI is a developing area of research. The presented in vitro results confirm that all three metabolites are potent inhibitors of CYP3A4 with unbound  $IC_{50}$  values in the nanomolar range, comparable to itraconazole  $IC_{50}$  (Fig. 3; Table 4). When the ratio between circulating metabolite concentrations and  $K_i$  is higher than 0.1, PBPK modeling is recommended (Callegari et al., 2013). All itraconazole metabolites were predicted to have values of the ratio between circulating metabolite concentrations and  $K_i$  above 0.1 and to significantly contribute to the observed clinical DDIs by Templeton et al. (2008). Therefore, it can be considered highly relevant to build a PBPK

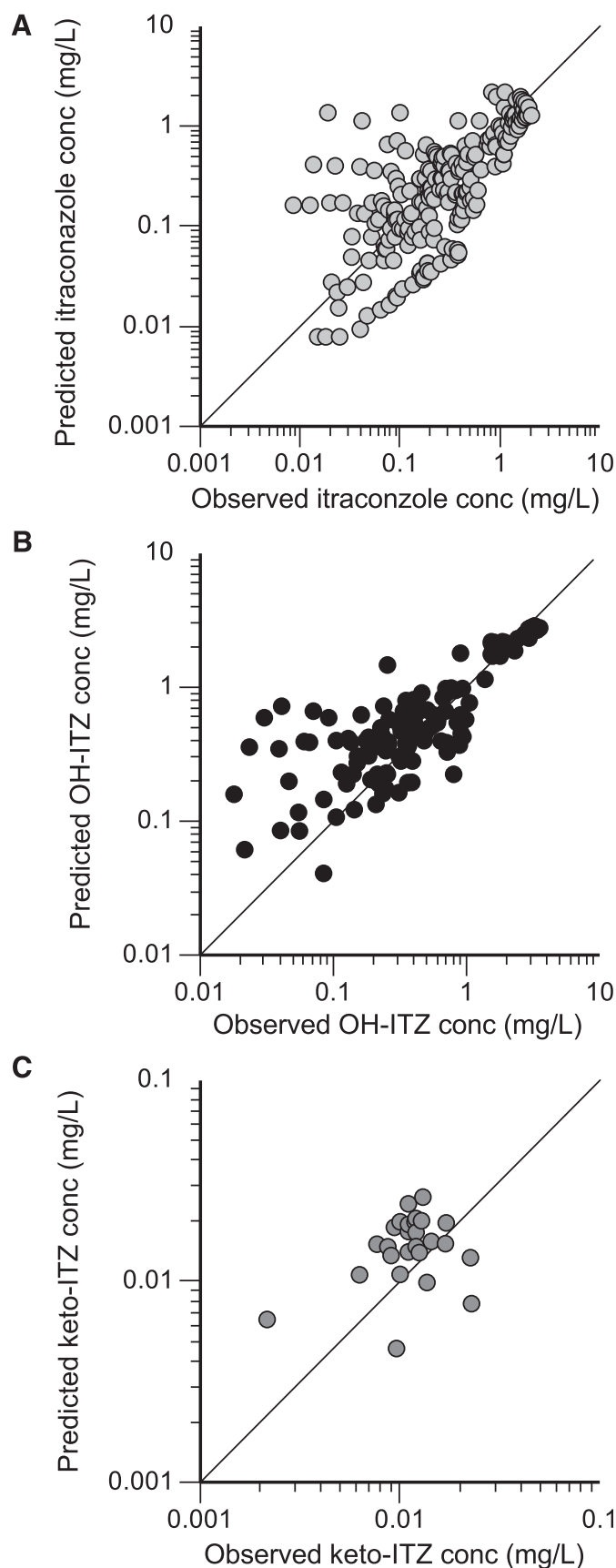


**Fig. 7.** Plasma concentrations predicted vs. observed at the same time points for itraconazole (A), OH-ITZ (B), and keto-ITZ (C). The black line represents the line of unity.

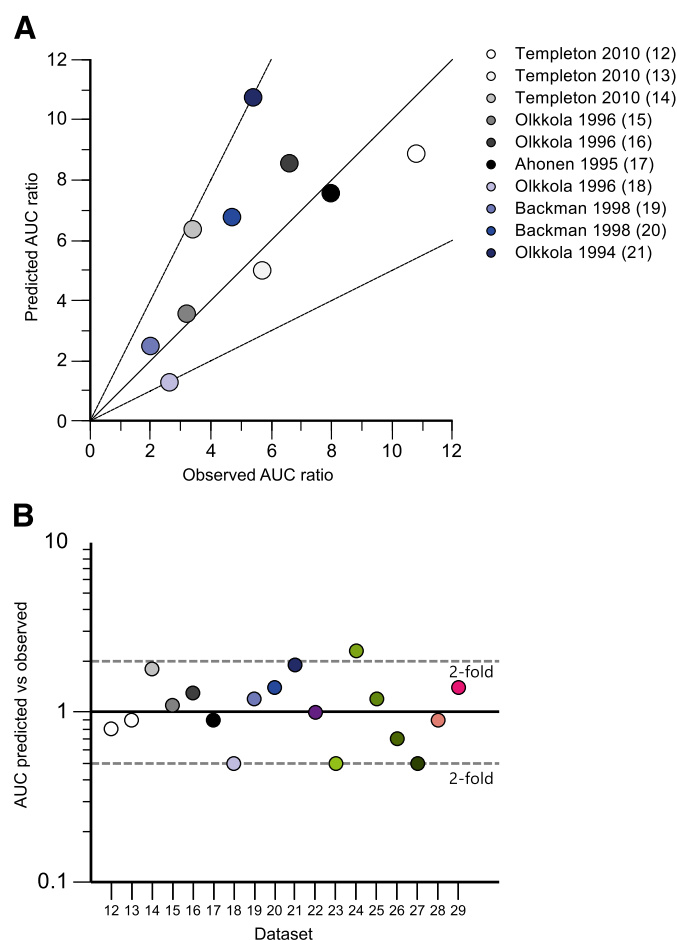


**Fig. 8.** Predicted vs. observed mean AUC ratio: (A) midazolam when coadministered with itraconazole for 10 clinical DDI studies; (B) including midazolam and other CYP3A4 substrates. Each study is represented by a circle; details of the study design can be found in Table 2. The solid line represents the line of unity and the dotted line represents the 2-fold error.

model that includes all metabolites, and in this paper we have presented the first step that includes the two first metabolites that are sequentially formed: OH-ITZ and keto-ITZ. The current model enables simulations for hypothesis testing to gain a deeper understanding of the contribution of the metabolites to the observed DDI (Fig. 9). The relative contribution depends on the time window observed after dosing; therefore, this model also enables simulations of the metabolite profiles over time with different trial designs. The relative role of OH-ITZ is increased with time after itraconazole dosing, being similarly important to itraconazole after 12 hours and having even higher contribution after day 3. However, the contribution of keto-ITZ is minor (<5%) over time. Hence, this is the first study by PBPK modeling that assesses in detail the contribution of keto-ITZ and establishes the low impact to the overall inhibition. Nevertheless, the inclusion of this metabolite in the model is indispensable to allow further development including ND-ITZ, which is expected to play a more significant role in the inhibition 12 hours or more following the last dose of itraconazole. Given the long half-life, lower protein binding, and potency of ND-ITZ, it can be predicted that its contribution to the observed DDI is increasing with time (similar to OH-ITZ) and this will be crucial when the CYP3A4 substrate is given more than 12 hours or days after the last dose of itraconazole. Thus, the next step will be to also include the third metabolite (ND-ITZ) to further improve the DDI prediction in those scenarios.

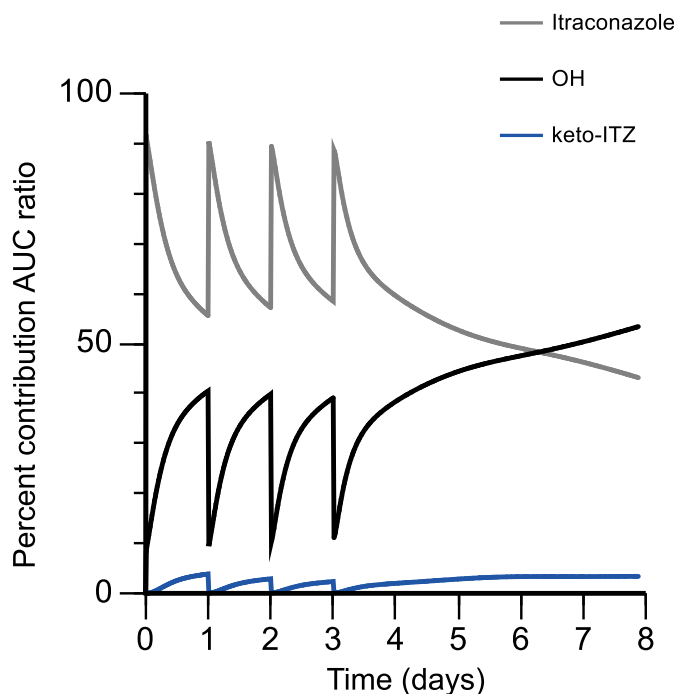


**Fig. 9.** Predicted percent contribution of itraconazole, and its metabolites (OH-ITZ and keto-ITZ), to the AUC ratio observed in the clinical DDI. Itraconazole (gray), OH-ITZ (black), and keto-ITZ (blue). Simulations with the PBPK model correspond to the administration of itraconazole 200 mg once daily during 4 days in capsules formulated under fasted conditions assuming that the AUC ratio can be fully explained by the inhibition of itraconazole, OH-ITZ, and keto-ITZ, but not by other metabolites such as ND-ITZ.

Previous reports (Chen et al., 2016; Liu et al., 2016) have emphasized discrepancies in reported *in vitro* data. For example, a 30-fold range of values has been reported for  $f_{u,p}$  in plasma for the parent compound (Heykants et al., 1989; Arredondo et al., 1995, 1999; Ishigam et al., 2001; Templeton et al., 2008). A second example is the reported  $K_i$  or  $IC_{50}$  values that vary between 150- and 170-fold for itraconazole and OH-ITZ, respectively (Back and Tjia, 1991; von Moltke et al., 1996; Wang et al., 1999; Ishigam et al., 2001; Tran et al., 2002; Isoherranen et al., 2004). As mentioned previously, high-quality *in vitro* data are critical when building a mechanistic bottom-up PBPK model (Jamei et al., 2009), and this is emphasized as well by our sensitivity analysis results (Fig. 6). Therefore, key parameters were experimentally determined in the same laboratory at the same occasion for the parent and the metabolites. In this report, data are generally presented with good precision on different experimental days ( $CV\% < 30$ ), increasing the confidence in our data. At the same time, the *in vitro-in vivo* extrapolation and modeling done validate the *in vitro* data herein generated since the observed clinical PK and DDI were recovered for itraconazole and its metabolites. In the new draft US Food and Drug Administration *in vitro* DDI guideline it is recommended to use a  $f_{u,p}$  value of 0.01 for mechanistic modeling even though lower values have been experimentally determined (CDER, 2017b). The reason is the high uncertainty with lower measured values for highly bound compounds. Given the uncertainties of the *in vitro* measured plasma protein binding, the value recommended by US Food and Drug Administration was used.

The scope for this study was to mechanistically describe the most critical processes for assessing the CYP3A4 inhibition of itraconazole and its metabolites by *in vitro-in vivo* extrapolation, but it goes without saying that other questions remain to be studied. The contribution of the third metabolite, ND-ITZ, to DDI has been suggested as being clinically relevant (Templeton et al., 2008), but our model does not include it due

to limitations of the software. However, *in vitro* data for ND-ITZ were generated during this study to enable future model development. There are conflicting data on hepatic uptake for itraconazole (Yamano et al., 1999; Higgins et al., 2014). In the current model hepatic uptake was set to 1 following the most recent publication, which showed lack of hepatic uptake in *in vitro* human primary hepatocytes and knockout mice. However, it could be beneficial to further investigate this to clarify the possibility that carrier-mediated transport might be involved. It is also important to remember that itraconazole and its metabolites are known inhibitors of P-gp and other transporters (Vermeer et al., 2016). The absorption of itraconazole is currently described by first-order kinetics. This limits the simulations on the potential regional differences in the inhibition of intestinal CYP3A4 and transporters. Expansion to a multicompartment gut model is something that could be evaluated and possibly included in future model versions to further improve the mechanistic behavior of the model.

In this paper, a model is presented in which we have successfully included the metabolite keto-ITZ into a PBPK model for itraconazole PK that enables DDI simulations. We believe that this model provides improved mechanistic understanding of the PK and DDI of ITZ and its metabolites. The results presented and sensitivity analyses highlight the importance of having robust *in vitro* and *in vivo* data to enable complex model building. The predictive DDI risk capability of this model is improved compared with the Simcyp itraconazole library model (100% vs. 80% predicted within 2-fold), showing no bias and good precision. Therefore, our observations suggest that this novel PBPK model built for itraconazole and two of its main metabolites can be successfully used to both evaluate DDI involving new victim compounds and to facilitate optimal study design.

#### Acknowledgments

We thank Dr. Martin Hayes at AstraZeneca for reviewing the manuscript. We also thank Danxi Li and Hongwen Du at Pharmaron and the Wave1 Drug Metabolism and Pharmacokinetics Department at AstraZeneca for providing experimental assistance.

#### Authorship Contributions

*Participated in research design:* Prieto Garcia, Kanebratt, Ericsson, Lennernäs, Lundahl.

*Conducted experiments:* Prieto Garcia.

*Performed data analysis:* Prieto Garcia, Janzén, Lundahl.

*Wrote or contributed to the writing of the manuscript:* Prieto Garcia, Janzén, Kanebratt, Ericsson, Lennernäs, Lundahl.

#### References

- Ahonen J, Olkkola KT, and Neuvonen PJ (1995) Effect of itraconazole and terbinafine on the pharmacokinetics and pharmacodynamics of midazolam in healthy volunteers. *Br J Clin Pharmacol* **40**:270–272.
- Arredondo G, Calvo R, Marcos F, Martínez-Jordá R, and Suarez E (1995) Protein binding of itraconazole and fluconazole in patients with cancer. *Int J Clin Pharmacol Ther* **33**:449–452.
- Arredondo G, Suárez E, Calvo R, Vazquez JA, García-Sánchez J, and Martínez-Jordá R (1999) Serum protein binding of itraconazole and fluconazole in patients with diabetes mellitus. *J Antimicrob Chemother* **43**:305–307.
- Back DJ and Tjia JF (1991) Comparative effects of the antimycotic drugs ketoconazole, fluconazole, itraconazole and terbinafine on the metabolism of cyclosporin by human liver microsomes. *Br J Clin Pharmacol* **32**:624–626.
- Backman JT, Kivistö KT, Olkkola KT, and Neuvonen PJ (1998) The area under the plasma concentration-time curve for oral midazolam is 400-fold larger during treatment with itraconazole than with rifampicin. *Eur J Clin Pharmacol* **54**:53–58.
- Barone JA, Koh JG, Bierman RH, Colaizzi JL, Swanson KA, Gaffar MC, Moskovitz BL, Mechlini W, and Van de Velde V (1993) Food interaction and steady-state pharmacokinetics of itraconazole capsules in healthy male volunteers. *Antimicrob Agents Chemother* **37**:778–784.
- Barone JA, Moskovitz BL, Guarnieri J, Hassell AE, Colaizzi JL, Bierman RH, and Jessen L (1998) Food interaction and steady-state pharmacokinetics of itraconazole oral solution in healthy volunteers. *Pharmacotherapy* **18**:295–301.
- Benet LZ, Broccatelli F, and Oprea TI (2011) BDDCS applied to over 900 drugs. *AAPS J* **13**: 519–547.
- Bonate PL (2011) *Pharmacokinetic-Pharmacodynamic Modeling and Simulation*, 2nd ed, Springer, New York.

- Buchkowsky SS, Partovi N, and Ensom MH (2005) Clinical pharmacokinetic monitoring of itraconazole is warranted in only a subset of patients. *Ther Drug Monit* **27**:322–333.
- Callegari E, Kalgutkar AS, Leung L, Scott Obach R, Plowchalk DR, and Tse S (2013) Drug Metabolites as Cytochrome P450 inhibitors: A Retrospective Analysis and Proposed Algorithm for Evaluation of the Pharmacokinetic Interaction Potential of Metabolites in Drug Discovery and Development. *Drug Metab Dispos* **41**:2047–2055.
- Center for Drug Evaluation and Research (CDER) (2013) *Drug Safety Communication: FDA Limits Usage of Nizoral (Ketoconazole) Oral Tablets Due to Potentially Fatal Liver Injury and Risk of Drug Interactions and Adrenal Gland Problems*, U.S. Food and Drug Administration, Silver Spring, MD.
- Center for Drug Evaluation and Research (CDER) (2017a) *Guidance for Industry: Drug Interaction Studies—Study Design, Data Analysis and Clinical Implications*, U.S. Food and Drug Administration, Silver Spring, MD.
- Center for Drug Evaluation and Research (CDER) (2017b) *Guidance for Industry: In Vitro Metabolism- and Transporter-Mediated Drug-Drug Interaction Studies*, U.S. Food and Drug Administration, Silver Spring, MD.
- Cer RZ, Mudunuri U, Stephens R, and Lebeda FJ (2009)  $IC_{50}$ -to- $K_i$ : a web-based tool for converting  $IC_{50}$  to  $K_i$  values for inhibitors of enzyme activity and ligand binding. *Nucleic Acids Res* **37**:W441–W445.
- Chen S, Prieto Garcia L, Bergström F, Nordell P, and Grime K (2017) Intrinsic clearance assay incubational binding: a method comparison. *Drug Metab Dispos* **45**:342–345.
- Chen Y, Ma F, Lu T, Budha N, Jin JY, Kenny JR, Wong H, Hop CE, and Mao J (2016) Development of a physiologically based pharmacokinetic model for itraconazole pharmacokinetics and drug–drug interaction prediction. *Clin Pharmacokinet* **55**:735–749.
- Committee for Medicinal Products for Human Use (CHMP) (2013) *Press Release: European Medicines Agency Recommends Suspension of Marketing Authorisations for Oral Ketoconazole. EMA/458028/2013*, European Medicines Agency, London.
- Gertz M, Cartwright CM, Hobbs MJ, Kenworthy KE, Rowland M, Houston JB, and Galetin A (2013) Cyclosporine inhibition of hepatic and intestinal CYP3A4, uptake and efflux transporters: application of PBPK modeling in the assessment of drug–drug interaction potential. *Pharm Res* **30**:761–780.
- Hardin TC, Graybill JR, Fetchick R, Woestenborghs R, Rinaldi MG, and Kuhn JG (1988) Pharmacokinetics of itraconazole following oral administration to normal volunteers. *Antimicrob Agents Chemother* **32**:1310–1313.
- Heykants J, Van Peer A, Van de Velde V, Van Rooy P, Meuldermans W, Lavrijsen K, Woestenborghs R, Van Cutsem J, and Cauwenbergh G (1989) The clinical pharmacokinetics of itraconazole: an overview. *Mycoses* **32** (Suppl 1):67–87.
- Higgins JW, Ke AB, and Zamek-Gliszczynski MJ (2014) Clinical CYP3A inhibitor alternatives to ketoconazole, clarithromycin and itraconazole, are not transported into the liver by hepatic organic anion transporting polypeptides and organic cation transporter 1. *Drug Metab Dispos* **42**:1780–1784.
- Ishigami M, Uchiyama M, Kondo T, Iwabuchi H, Inoue S, Takasaki W, Ikeda T, Komai T, Ito K, and Sugiyama Y (2001) Inhibition of in vitro metabolism of simvastatin by itraconazole in humans and prediction of in vivo drug–drug interactions. *Pharm Res* **18**:622–631.
- Isoherranen N, Kunze KL, Allen KE, Nelson WL, and Thummel KE (2004) Role of itraconazole metabolites in CYP3A4 inhibition. *Drug Metab Dispos* **32**:1121–1131.
- Jamei M, Dickinson GL, and Rostami-Hodjegan A (2009) A framework for assessing inter-individual variability in pharmacokinetics using virtual human populations and integrating general knowledge of physical chemistry, biology, anatomy, physiology and genetics: a tale of ‘bottom-up’ vs ‘top-down’ recognition of covariates. *Drug Metab Pharmacokinet* **24**:53–75.
- Jones HM, Chen Y, Gibson C, Heimbach T, Parrott N, Peters SA, Snoeys J, Upreti VV, Zheng M, and Hall SD (2015) Physiologically based pharmacokinetic modeling in drug discovery and development: a pharmaceutical industry perspective. *Clin Pharmacol Ther* **97**:247–262.
- Kaukonen KM, Olkkola KT, and Neuvonen PJ (1997) Itraconazole increases plasma concentrations of quinine. *Clin Pharmacol Ther* **62**:510–517.
- Liang X, Van Parys M, Ding X, Zeng N, Bi L, Dorshort D, McKnight J, Milanowski D, Mao J, Chen Y, et al. (2016) Simultaneous determination of itraconazole, hydroxy itraconazole, keto itraconazole and N-desalkyl itraconazole concentration in human plasma using liquid chromatography with tandem mass spectrometry. *J Chromatogr B Anal Technol Biomed Life Sci* **1020**:111–119.
- Liu L, Bello A, Dresser MJ, Heald D, Komjathy SF, O’Mara E, Rogge M, Stoch SA, and Robertson SM (2016) Best practices for the use of itraconazole as a replacement for ketoconazole in drug–drug interaction studies. *J Clin Pharmacol* **56**:143–151.
- Marsousi N, Desmeules JA, Rudaz S, and Daali Y (2018) Prediction of drug–drug interactions using physiologically-based pharmacokinetic models of CYP450 modulators included in Simcyp software. *Biopharm Drug Dispos* **39**:3–17.
- Marston SA and Polli JE (1997) Evaluation of direct curve comparison metrics applied to pharmacokinetic profiles and relative bioavailability and bioequivalence. *Pharm Res* **14**:1363–1369.
- Miura M, Takahashi N, Nara M, Fujishima N, Kagaya H, Kameoka Y, Saitoh H, Tagawa H, and Sawada K (2010) A simple, sensitive high-performance liquid chromatography–ultraviolet method for the quantification of concentration and steady-state pharmacokinetics of itraconazole and hydroxyitraconazole. *Ann Clin Biochem* **47**:432–439.
- Mouton JW, van Peer A, de Beule K, Van Vliet A, Donnelly JP, and Soons PA (2006) Pharmacokinetics of Itraconazole and Hydroxyitraconazole in Healthy Subjects after Single and Multiple Doses of a Novel Formulation. *Antimicrob Agents Chemother* **50**:4096–4102.
- Nestorov IA (1999) Sensitivity analysis of pharmacokinetic and pharmacodynamic systems: I. A structural approach to sensitivity analysis of physiologically based pharmacokinetic models. *J Pharmacokinet Biopharm* **27**:577–596.
- Neuvonen PJ, Kantola T, and Kivistö KT (1998) Simvastatin but not pravastatin is very susceptible to interaction with the CYP3A4 inhibitor itraconazole. *Clin Pharmacol Ther* **63**:332–341.
- Neuvonen PJ, Varhe A, and Olkkola KT (1996) The effect of ingestion time interval on the interaction between itraconazole and triazolam. *Clin Pharmacol Ther* **60**:326–331.
- Ohkubo T and Osanai T (2005) Determination of itraconazole in human plasma by high-performance liquid chromatography with solid-phase extraction. *Ann Clin Biochem* **42**:94–98.
- Oie S and Tozer TN (1979) Effect of altered plasma protein binding on apparent volume of distribution. *J Pharm Sci* **68**:1203–1205.
- Olkkola KT, Ahonen J, and Neuvonen PJ (1996) The effects of the systemic antimycotics, itraconazole and fluconazole, on the pharmacokinetics and pharmacodynamics of intravenous and oral midazolam. *Anesth Analg* **82**:511–516.
- Olkkola KT, Backman JT, and Neuvonen PJ (1994) Midazolam should be avoided in patients receiving the systemic antimycotics ketoconazole or itraconazole. *Clin Pharmacol Ther* **55**:481–485.
- Poirier JM and Cheymol G (1998) Optimisation of itraconazole therapy using target drug concentrations. *Clin Pharmacokinet* **35**:461–473.
- Poulin P and Theil FP (2009) Development of a novel method for predicting human volume of distribution at steady-state of basic drugs and comparative assessment with existing methods. *J Pharm Sci* **98**:4941–4961.
- Rostami-Hodjegan A (2012) Physiologically based pharmacokinetics joined with in vitro-in vivo extrapolation of ADME: a marriage under the arch of systems pharmacology. *Clin Pharmacol Ther* **92**:50–61.
- Rostami-Hodjegan A, Tamai I, and Pang KS (2012) Physiologically based pharmacokinetic (PBPK) modeling: it is here to stay! *Biopharm Drug Dispos* **33**:47–50.
- Rowland M, Peck C, and Tucker G (2011) Physiologically-based pharmacokinetics in drug development and regulatory science. *Annu Rev Pharmacol Toxicol* **51**:45–73.
- Sager JE, Yu J, Ragueneau-Majlessi I, and Isoherranen N (2015) Physiologically based pharmacokinetic (PBPK) modeling and simulation approaches: a systematic review of published models, applications, and model verification. *Drug Metab Dispos* **43**:1823–1837.
- Sjögren E, Lennernäs H, Andersson TB, Gräsjö J, and Bredberg U (2009) The multiple depletion curves method provides accurate estimates of intrinsic clearance ( $CL_{int}$ ), maximum velocity of the metabolic reaction ( $V_{max}$ ), and Michaelis constant ( $K_m$ ): accuracy and robustness evaluated through experimental data and Monte Carlo simulations. *Drug Metab Dispos* **37**:47–58.
- Sjögren E, Westergren J, Grant I, Hanisch G, Lindfors L, Lennernäs H, Abrahamsson B, and Tannergren C (2013) In silico predictions of gastrointestinal drug absorption in pharmaceutical product development: application of the mechanistic absorption model GI-Sim. *Eur J Pharm Sci* **49**:679–698.
- Templeton I, Peng CC, Thummel KE, Davis C, Kunze KL, and Isoherranen N (2010) Accurate prediction of dose-dependent CYP3A4 inhibition by itraconazole and its metabolites from in vitro inhibition data. *Clin Pharmacol Ther* **88**:499–505.
- Templeton IE, Thummel KE, Kharasch ED, Kunze KL, Hoffer C, Nelson WL, and Isoherranen N (2008) Contribution of itraconazole metabolites to inhibition of CYP3A4 in vivo. *Clin Pharmacol Ther* **83**:77–85.
- Tran TH, Von Moltke LL, Venkatakrishnan K, Granda BW, Gibbs MA, Obach RS, Harmatz JS, and Greenblatt DJ (2002) Microsomal protein concentration modifies the apparent inhibitory potency of CYP3A inhibitors. *Drug Metab Dispos* **30**:1441–1445.
- Tsamandouras N, Rostami-Hodjegan A, and Aarons L (2015) Combining the ‘bottom up’ and ‘top down’ approaches in pharmacokinetic modelling: fitting PBPK models to observed clinical data. *Br J Clin Pharmacol* **79**:48–55.
- Uno T, Shimizu M, Sugawara K, and Tateishi T (2006) Sensitive determination of itraconazole and its active metabolite in human plasma by column-switching high-performance liquid chromatography with ultraviolet detection. *Ther Drug Monit* **28**:526–531.
- Van Peer A, Woestenborghs R, Heykants J, Gasparini R, and Gauwenbergh G (1989) The effects of food and dose on the oral systemic availability of itraconazole in healthy subjects. *Eur J Clin Pharmacol* **36**:423–426.
- Varhe A, Olkkola KT, and Neuvonen PJ (1994) Oral triazolam is potentially hazardous to patients receiving systemic antimycotics ketoconazole or itraconazole. *Clin Pharmacol Ther* **56**:601–607.
- Vermeer LM, Isringhausen CD, Ogilvie BW, and Buckley DB (2016) Evaluation of ketoconazole and its alternative clinical CYP3A4/5 inhibitors as inhibitors of drug transporters: the in vitro effects of ketoconazole, ritonavir, clarithromycin, and itraconazole on 13 clinically-relevant drug transporters. *Drug Metab Dispos* **44**:453–459.
- von Moltke LL, Greenblatt DJ, Schmider J, Duan SX, Wright CE, Harmatz JS, and Shader RI (1996) Midazolam hydroxylation by human liver microsomes in vitro: inhibition by fluoxetine, norfluoxetine, and by azole antifungal agents. *J Clin Pharmacol* **36**:783–791.
- Wagner C, Jantravid E, Kesiosoglou F, Vertzoni M, Reppas C, and B Dressman J (2012) Predicting the oral absorption of a poorly soluble, poorly permeable weak base using biorelevant dissolution and transfer model tests coupled with a physiologically based pharmacokinetic model. *Eur J Pharm Biopharm* **82**:127–138.
- Wan H and Rehngren M (2006) High-throughput screening of protein binding by equilibrium dialysis combined with liquid chromatography and mass spectrometry. *J Chromatogr A* **1102**:125–134.
- Wang JS, Wen X, Backman JT, Taavitsainen P, Neuvonen PJ, and Kivistö KT (1999) Midazolam  $\alpha$ -hydroxylation by human liver microsomes in vitro: inhibition by calcium channel blockers, itraconazole and ketoconazole. *Pharmacol Toxicol* **85**:157–161.
- Wang YH, Jones DR, and Hal SD (2004) Prediction of cytochrome P450 3A inhibition by verapamil enantiomers and their metabolites. *Drug Metab Dispos* **32**:259–266.
- Yamano K, Yamamoto K, Kotaki H, Sawada Y, and Iga T (1999) Quantitative prediction of metabolic inhibition of midazolam by itraconazole and ketoconazole in rats: implication of concentrative uptake of inhibitors into liver. *Drug Metab Dispos* **27**:395–402.
- Yasui N, Kondo T, Otani K, Furukori H, Kaneko S, Ohkubo T, Nagasaki T, and Sugawara K (1998) Effect of itraconazole on the single oral dose pharmacokinetics and pharmacodynamics of alprazolam. *Psychopharmacology (Berl)* **139**:269–273.
- Yoo SD, Kang E, Jun H, Shin BS, Lee KC, and Lee KH (2000) Absorption, first-pass metabolism, and disposition of itraconazole in rats. *Chem Pharm Bull (Tokyo)* **48**:798–801.

**Address correspondence to:** Luna Prieto Garcia, Drug Metabolism and Pharmacokinetics; Cardiovascular and Metabolic Diseases, IMED Biotech Unit, AstraZeneca, Gothenburg, Sweden. E-mail: luna.prietogarcia@astrazeneca.com